Polycrystalline MnBi as a transverse thermoelectric material

AIP Advances

Polycrystalline MnBi as a transverse thermoelectric material

Cite as: AIP Advances **13**, 035231 (2023); https://doi.org/10.1063/5.0135578
Submitted: 30 November 2022 • Accepted: 05 March 2023 • Published Online: 21 March 2023

A. Sola, E. S. Olivetti, L. Martino, et al.

Polycrystalline MnBi as a transverse thermoelectric material

Cite as: AIP Advances 13, 035231 (2023); doi: 10.1063/5.0135578
Submitted: 30 November 2022 • Accepted: 5 March 2023 •
Published Online: 21 March 2023

A. Sola,[a] E. S. Olivetti, L. Martino, and V. Basso

AFFILIATIONS

Istituto Nazionale di Ricerca Metrologica, Strada delle Cacce 91, 10135 Turin, Italy

[a]Author to whom correspondence should be addressed: a.sola@inrim.it

ABSTRACT

To assess the potential of polycrystalline MnBi as a transverse thermoelectric material, we have experimentally investigated its anomalous Nernst effect (ANE) by means of the heat flux method. We prepared MnBi samples by powder metallurgy; this technique allows the preparation of samples in arbitrary shapes with the possibility to tailor their magnetic properties. In the material exhibiting the highest remanent magnetization, we found a value of the ANE thermopower of −1.1 μV/K at 1 T, after the compensation of the ordinary Nernst effect from pure bismuth present inside the polycrystalline sample. This value is comparable with those reported in the literature for single crystals.

The performance of a thermoelectric device working with the Seebeck/Peltier effects is ruled by both its architecture and the characteristics of the materials. The latter is represented by the dimensionless figure of merit $ZT = \varepsilon^2\sigma T/k$, where ε is the Seebeck thermopower, σ is the electrical conductivity, T is the temperature, and k is the thermal conductivity. The typical device architecture consists of pillars of p- and n-type semiconductors that are thermally in parallel and electrically in series.[1] This configuration allows the maximization of efficiency, but limits the possibilities of arbitrary shaping. Structures, such as thermal-sensing coatings[2] or flexible devices,[3] can however be devised by exploiting transverse thermoelectric effects,[4] also called thermomagnetic effects.[5] The Nernst effect refers to the transverse thermopower $N = \nabla_y V/\nabla_x T$ that rises in a material in which the temperature gradient $\nabla_x T$ is applied in the presence of a magnetic field B_z. In ferromagnetic materials, with spontaneous magnetization, the thermopower is called spontaneous or anomalous Nernst effect (ANE). The performance of a thermomagnetic device depends on the ratio between two lengths: one along the electric potential and the other along the thermal gradient. These are oriented along perpendicular directions, while in a Seebeck/Peltier device, the two lengths are parallel and coincide. This fact opens up new possibilities for the improvement of the performance, along with more freedom in the geometries, by tuning the dimensions and shapes of the devices. The optimum shape, for an architecture based on multistage cascading, was derived by Harman[6] and subsequently developed.[7–9] The opportunity to adapt the shape of thermoelectric devices to the geometries of existing systems is of paramount importance and sometimes it is the only option, for example, for the proposal of self-cooling cables.[10] In this framework, the study of thermomagnetic effects in ferromagnets that could be easily produced in different sizes and shapes, such as polycrystalline materials, becomes crucial. A material worth investigating is MnBi, which allows the preparation of magnetic samples by powder metallurgy processes. The thermomagnetic properties of MnBi single crystals have been recently investigated,[11] with some interesting findings in terms of an extra contribution to the transverse thermopower. This originates from magnon–electron interaction due to the large spin–orbit coupling of the MnBi itself and it was also observed in heterogeneous systems, such as multi-layers[12,13] and composites of bulk materials, with heavy metal nanoparticles.[14] Nevertheless, the possibility of exploiting this favorable condition in a single material makes the MnBi appealing in the framework of the thermomagnetic applications. Previous studies on MnBi single-crystals report a transverse thermopower at the saturating field of 2 μV/K at room temperature and 10 μV/K at 80 K.[11] These values are comparable with the maximum ANE thermopowers reported in

a recent perspective paper by Uchida *et al.*,[15] where the highest ANE coefficients are reported for the Heusler ferromagnet Co_2MnGa. Some experimental results of ANE in polycrystalline samples are already present in the literature, with large values at 2 T recently reported for polycrystalline Fe_xGa_{4-x} ($2.96 < x < 3.15$).[16]

The aim of this study is the investigation of the ANE thermopower in polycrystalline MnBi samples prepared by powder metallurgy processes. Our study has the scope to unveil the gap in performance between ideal materials used for the study of fundamental phenomena and less ordered systems, with the advantage, in this second category, to exploit the hard magnetic properties of MnBi and have a device working without an external applied magnetic field. Samples were prepared through a powder metallurgy route that consists in the annealing of manganese and bismuth powders, previously mixed and pressed to form a pellet. All the powders were handled in a nitrogen-filled glove box to avoid oxidation. The α-MnBi phase is obtained by heating at 320 °C for 1 h in a vacuum or inert atmosphere. We prepared three types of samples, exploiting magnetic field annealing and the induction of defects by means of high-energy ball milling to tailor the microstructure and hence the magnetic properties of the samples.[17] The hysteresis loops of the samples prepared according to these three procedures, measured by means of vibrating sample magnetometry (VSM), are shown in Fig. 1. Sample A, which can be considered as a reference, has been annealed in a vacuum without an applied magnetic field; this preparation favored the formation of randomly oriented and well-developed MnBi grains. Sample B was annealed in a nitrogen atmosphere under a static magnetic field of 1 T produced by a Halbach cylinder. This procedure allows the development of a preferred orientation of the MnBi grains with their c-axis along the applied field direction. The resulting hysteresis cycle shows larger saturation and higher remanent magnetization compared to the reference sample. For sample C, we focused on the development of coercivity. In order to obtain a high value, we milled the material that was annealed in the same way as sample A in a planetary ball mill. The milling process was for 1 h at 450 rpm in a zirconia jar (ball-to-powder ratio ~14), and afterward we pressed the resulting powder in a new pellet. Smaller grain size and the presence of defects,

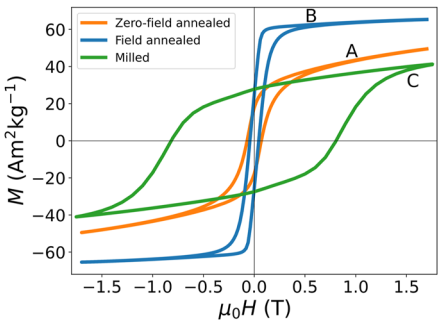

FIG. 1. Magnetization as a function of the applied magnetic field measured by vibrating sample magnetometry (VSM) for each type of polycrystalline MnBi sample. A: isotropic reference sample obtained by annealing without applied magnetic field. B: sample annealed under a static 1 T magnetic field. C: Sample obtained by milling of the reference sample.

representing pinning centers for domain wall motion, allowed to increase the value of the coercive field significantly,[17] as shown in Fig. 1. The transverse thermopower of the aforementioned samples was investigated by an experimental setup based on the heat flux method. This procedure allows us to disregard the thermal resistances between the sample and the thermal sensors, which usually affects the direct measurement of the temperature difference. The heat flux method consists in an electric characterization of a sample under test as a function of the heat flux traversing it. This last quantity is generated by a pair of Peltier modules: the bottom surfaces of each module are connected to a thermal reservoir whose temperature is set by a temperature control system. The top surfaces are connected to two brass blocks that are the cold and hot baths; these clamp a second pair of Peltier cells between which the sample is placed. These cells directly connected to the sample work as sensors, and they are calibrated with a Joule resistor according to a procedure reported in previous studies;[18,19] the characteristic that we found in the present work is 1.07 V/W for both the Peltier sensors. In order to avoid uncontrolled heat leakages, the whole system is kept under vacuum (10^{-7} mbar) and the electric connections to the sample are made with gold wires with a diameter of 0.012 mm. This experimental approach provides the values of the heat current density j_q and voltage drop across the sample V_{ANE} that are found in the expression of the ANE thermopower N,

$$N = \frac{V_{ANE}/L_y}{-j_q/k}, \tag{1}$$

where L_y is the distance between the electrodes and k is the thermal conductivity of the material under investigation whose value, for our study, has been approximated to the one of pure bismuth that is 7.9 W K^{-1} m^{-1}. A scheme of the measurement configuration is shown in Fig. 2(a). The magnetic field is perpendicular to the directions of the voltage drop V_{ANE} and the one of the heat current density j_q. An electromagnet was used to apply the magnetic field alternating between ±1 T and measured by a calibrated Hall probe. We compensated the induced voltage that constitutes a spurious component of the measured voltage drop V_{ANE}; this component arose from the variation of the magnetic flux density across the electric wiring of the experiment. For each sample mounting inside the measurement system, the determination of these induced voltages was performed by applying the same varying magnetic field in the absence of heat fluxes. The results for the three types of MnBi samples are shown in Fig. 2(b). The ANE voltages V_{ANE}, as a function of the applied magnetic field, are shown in the top row of Fig. 2(b). Here, we represented only the values of V_{ANE} obtained with positive temperature differences, as an example of the measurement. The corresponding values of temperature difference are reported in the labels and have been derived as $\Delta T = -j_q L_x/k$. The measured voltage V_{ANE} follows a hysteresis loop whose magnitude increases along the vertical axis for higher temperature differences. The values of V_{ANE} at zero applied field, highlighted by black dots on the hysteresis loops in the top row of Fig. 2(b), correspond to a Nernst effect driven by the remanent magnetization of the sample. These values, normalized by the geometrical factors of the samples, are used to represent V_{ANE}/L_y at remanence as a function of the thermal gradients, shown in the bottom row of Fig. 2(b). Our system is able to produce heat currents j_q in both positive and negative directions

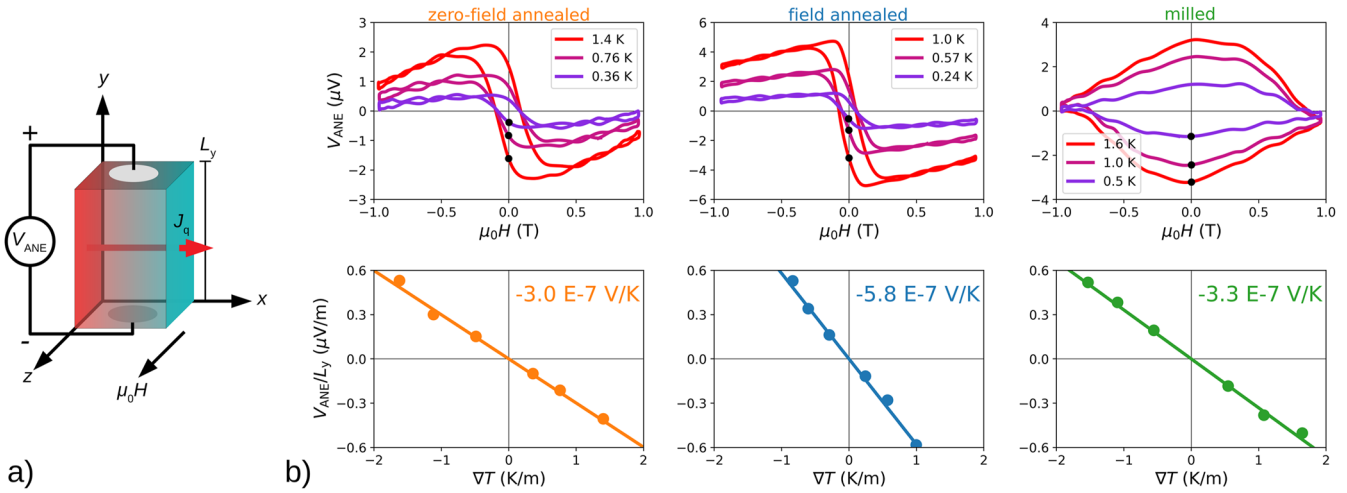

FIG. 2. (a) Geometry of the ANE measurements: the sample is heated along the x-axis, magnetized along the z-axis, and the V_{ANE} voltage is detected along the y-axis. The distance between electrodes is L_y. (b) Top: ANE voltages as a function of the applied magnetic field for three positive values of temperature difference. Bottom: gradients of ANE voltage as a function of the applied thermal gradient measured at zero magnetic fields (corresponding to the values highlighted by the black dots on the top graphs). In the labels, the values for the ANE thermopower are reported. Each column corresponds to the type of material: orange dataset for the zero-field annealed sample (A), blue dataset for the field annealed sample (B), and green dataset for the milled sample (C).

along x; this allows us to test the signs of the ANE voltages according to the signs of j_q. The slopes in Fig. 2(b) are the values of ANE thermopower at remanence. Sample B, prepared under magnetic field annealing (blue set), exhibits the largest value, $N = -5.8 \cdot 10^{-7}$ V/K. The curves shown in the top row of Fig. 2(b) resemble the VSM measurements in Fig. 1: particularly, samples B and C exhibit high remanent magnetization and high coercivity, respectively, also in their ANE characteristics. A decrease in the V_{ANE} for increasing applied magnetic fields is found in all samples; we interpret this phenomenon as due to the presence of unreacted bismuth, a source of transverse thermopower whose sign is opposite to the one of the MnBi ANE. Although there are other works about the thermomagnetic response of MnBi/Bi composites,[14,20] this feature has not been specifically investigated. However, a similar behavior of the V_{ANE} can be found in the transverse thermopower reported for MnBi and MnBi-Au composites.[14] In order to investigate this phenomenon in more detail, we measured the Nernst thermopower of a pure bismuth pellet obtained with the same experimental setup and in the same geometrical configuration used for the MnBi samples. The result of this measurement is reported in Fig. 3. The value of the Nernst coefficient of bismuth, $32 \cdot 10^{-6}$ V K^{-1} T^{-1}, has been derived by the plateau of the derivative of the curve of Fig. 3. The red line is a guide for the eye whose slope is equal to the Nernst coefficient of bismuth and, therefore, parallel to the thermopower vs field curve in the range above 1 T. The three main features of the measured Nernst effect of bismuth are the high magnitude, the sign, opposite to the one of the MnBi ANE thermopower, and the behavior as a function of the applied magnetic field, which is non-linear but exhibits no hysteresis. With this information, it is possible to analyze the MnBi ANE measured thermopower by taking into account the presence of the bismuth Nernst voltage and considering the total measured voltage as

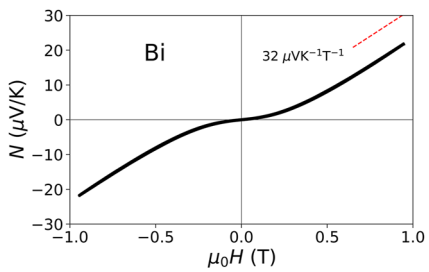

FIG. 3. Nernst thermopower of bismuth as a function of the applied magnetic field, normalized by the geometrical factors of the sample and by the thermal gradient. Experimental data are represented by the black line, while the red line is the reference slope for a Nernst coefficient of $32 \cdot 10^{-6}$ V K^{-1} T^{-1}.

$$V_{tot} = (1 - x_{Bi}) V_{MnBi} + x_{Bi} V_{Bi}, \quad (2)$$

where x_{Bi} is the unreacted bismuth linear phase fraction inside the sample, V_{Bi} is the Nernst voltage contribution from bismuth, and V_{MnBi} is the sought ANE voltage from MnBi. The criterion used to choose a value of x_{Bi} is to make the ANE loop follow the VSM loop for each type of material, by using the data reported in Fig. 3 for the V_{Bi}. According to this calculation, it is possible to obtain the MnBi ANE voltage V_{MnBi} extrapolated to the absence of bismuth. The bottom row of Fig. 4 shows the same VSM data of Fig. 1 (orange lines) superimposed to the MnBi thermopowers (purple points) after the compensation of the Nernst contribution from bismuth for the three types of materials. In the first two samples, we observe the same coercivity by thermopower and VSM measurements thanks to the good

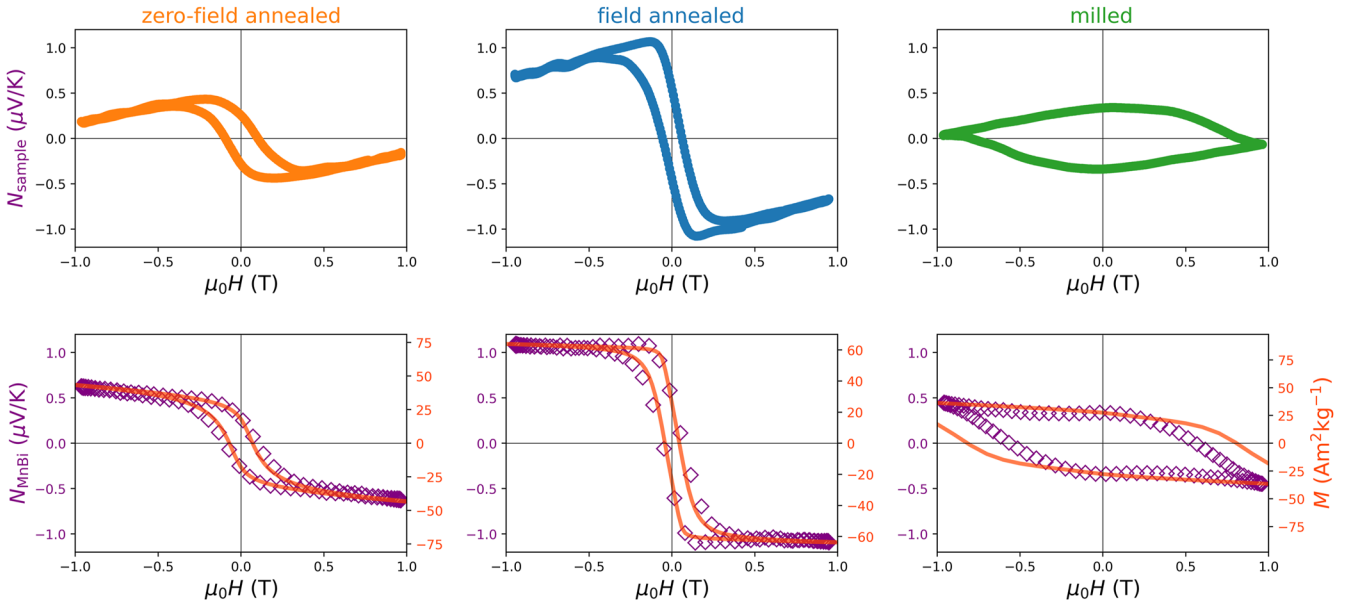

FIG. 4. Top: ANE thermopowers of MnBi samples as a function of the applied magnetic field, normalized by the geometrical factors. Bottom: A comparison between VSM magnetization curves (orange line) and ANE thermopowers of MnBi (purple diamonds) after the compensation of the Nernst effect of bismuth, originating from the unreacted phase inside the samples. The bismuth fractions needed to achieve the superimposition between the ANE and the VSM curves according to Eq. (2) is 2% for the zero-field annealed sample, 1.6% for the field annealed sample, and 1.6% for the milled sample.

superimposition of the data. For what concerns the third dataset, the milled sample, we observe a slight discrepancy between coercivity measured by VSM and ANE. This is due to the maximum field reachable by the ANE measurement system that is not strong enough to magnetize the sample as the VSM magnetometer. On the top row of Fig. 4 are reported the measured thermopowers from the samples, before the bismuth compensation. The results of the MnBi ANE thermopowers at remanence and at the saturating field after the bismuth compensation is summarized in Table I, for the three types of materials for which we report the values of coercivity. In the case of the field-annealed material (sample B), the value of ANE thermopower at 1 T reaches −1.1 μV/K, which is half of the value reported at room temperature for single crystal.[11] For the other types of materials (samples A and C), we observed lower ANE thermopowers. This is compatible with the anisotropic nature of the ANE, whose magnitude depends on the direction of the magnetization and of the c-axis of the MnBi crystals. We have further checked the value of the unreacted volume bismuth fraction by differential scanning calorimetry (DSC) measurements. The volume percentages of bismuth that we obtained were three to ten times bigger than the percentages needed to achieve the superimposition between the ANE thermopower curves and the magnetization curves of Fig. 4 (bottom). However, it is reasonable that the MnBi and the bismuth phases do not grow with the same shapes since the residual bismuth is presumably an intergranular phase that surrounds the MnBi crystals. With this model of the microstructure, it is possible to evaluate the linear phase fraction x_{Bi} as the amount of phase crossed by a line oriented along an arbitrary direction inside the MnBi sample. The result is compatible with the ones used to meet the condition of the superimposition between the magnetization curves and ANE thermopower curves.

TABLE I. ANE thermopowers of the materials under test.

MnBi sample	$\mu_0 H_c$ T	ANE at 0 T μV K^{-1}	ANE at 1 T μV K^{-1}
Zero-field annealed	0.08	−0.30	−0.63[a]
Field annealed	0.04	−0.58	−1.1[a]
Milled	0.80	−0.33	−0.45[a]

[a]ANE thermopower for the MnBi after the bismuth compensation, obtained from the data reported on the bottom row of Fig. 4.

In conclusion, we demonstrated the thermomagnetic characteristics of polycrystalline MnBi samples prepared by means of powder metallurgy followed by field annealing. This method permits easy manipulation of the magnetic properties at the preparation stage and its direct effect on the ANE thermopower. This work paves the way toward the optimization of the properties of a transverse thermoelectric material, such as MnBi: among the requirements, one of the most important is the high value of the remanent magnetization. Moreover, it is important to take into account the different contributions to the thermopower from materials whose thermomagnetic characteristics are different, as in the case of bismuth inside the MnBi samples. The optimization of these parameters allows the characteristics of polycrystalline samples to be comparable to the ones obtained from ideal and more difficult-to-produce materials, such as single crystals. This represents a step forward in the

applicability of thermomagnetic effects in the field of thermoelectric coolers and energy harvesting devices.

ACKNOWLEDGMENTS

The authors gratefully acknowledge the financial support of the Italian Ministry of University and Research (MUR) under the Next-Generation Metrology project.

AUTHOR DECLARATIONS

Conflict of Interest

The authors have no conflicts to disclose.

Author Contributions

A. Sola: Conceptualization (equal); Data curation (lead); Formal analysis (equal); Investigation (equal); Methodology (equal); Writing – original draft (lead); Writing – review & editing (lead). **E. Olivetti**: Conceptualization (equal); Data curation (supporting); Formal analysis (equal); Investigation (equal); Methodology (lead); Writing – original draft (supporting); Writing – review & editing (supporting). **L. Martino**: Methodology (supporting). **V. Basso**: Conceptualization (equal); Data curation (equal); Formal analysis (equal); Investigation (equal); Methodology (equal); Writing – original draft (equal); Writing – review & editing (equal).

DATA AVAILABILITY

The data that support the findings of this study are available from the corresponding author upon reasonable request.

REFERENCES

[1]F. J. DiSalvo, "Thermoelectric cooling and power generation," Science **285**, 703–706 (1999).
[2]A. Kirihara, K.-i. Uchida, Y. Kajiwara, M. Ishida, Y. Nakamura, T. Manako, E. Saitoh, and S. Yorozu, "Spin-current-driven thermoelectric coating," Nat. Mater. **11**, 686–689 (2012).
[3]A. Kirihara, K. Kondo, M. Ishida, K. Ihara, Y. Iwasaki, H. Someya, A. Matsuba, K. Uchida, E. Saitoh, N. Yamamoto , "Flexible heat-flow sensing sheets based on the longitudinal spin Seebeck effect using one-dimensional spin-current conducting films," Sci. Rep. **6**, 1–7 (2016).
[4]S. R. Boona, H. Jin, and S. Watzman, "Transverse thermal energy conversion using spin and topological structures," J. Appl. Phys. **130**, 171101 (2021).
[5]G. S. Nolas, J. Sharp, and J. Goldsmid, *Thermoelectrics: Basic Principles and New Materials Developments* (Springer Science & Business Media, 2001), Vol. 45.
[6]T. C. Harman, "Theory of the infinite stage Nernst-Ettingshausen refrigerator," Adv. Energy Convers. **3**, 667–676 (1963).
[7]C. F. Kooi, R. B. Horst, and K. F. Cuff, "Thermoelectric-thermomagnetic energy converter staging," J. Appl. Phys. **39**, 4257–4263 (1968).
[8]K. Scholz, P. Jandl, U. Birkholz, and Z. M. Dashevskii, "Infinite stage Ettingshausen cooling in Bi-Sb alloys," J. Appl. Phys. **75**, 5406–5408 (1994).
[9]M. M. H. Polash and D. Vashaee, "Infinite-stage Nernst-Ettingshausen cryocooler for practical applications," Phys. Rev. Appl. **15**, 014011 (2021).
[10]L. de'Medici, "Thermomagnetic mechanism for self-cooling cables," Phys. Rev. Appl. **5**, 024001 (2016).
[11]B. He, C. Şahin, S. R. Boona, B. C. Sales, Y. Pan, C. Felser, M. E. Flatté, and J. P. Heremans, "Large magnon-induced anomalous Nernst conductivity in single-crystal MnBi," Joule **5**, 3057–3067 (2021).
[12]K.-D. Lee, D.-J. Kim, H. Yeon Lee, S.-H. Kim, J.-H. Lee, K.-M. Lee, J.-R. Jeong, K.-S. Lee, H.-S. Song, J.-W. Sohn *et al.*, "Thermoelectric signal enhancement by reconciling the spin Seebeck and anomalous Nernst effects in ferromagnet/non-magnet multilayers," Sci. Rep. **5**, 10249 (2015).
[13]R. Ramos, T. Kikkawa, A. Anadón, I. Lucas, T. Niizeki, K. Uchida, P. A. Algarabel, L. Morellón, M. H. Aguirre, M. R. Ibarra, and E. Saitoh, "Interface-induced anomalous Nernst effect in Fe_3O_4/Pt-based heterostructures," Appl. Phys. Lett. **114**, 113902 (2019).
[14]S. R. Boona, K. Vandaele, I. N. Boona, D. W. McComb, and J. P. Heremans, "Observation of spin Seebeck contribution to the transverse thermopower in Ni-Pt and MnBi-Au bulk nanocomposites," Nat. Commun. **7**, 13714 (2016).
[15]K. Uchida, W. Zhou, and Y. Sakuraba, "Transverse thermoelectric generation using magnetic materials," Appl. Phys. Lett. **118**, 140504 (2021).
[16]Z. Feng, S. Minami, S. Akamatsu, A. Sakai, T. Chen, D. Nishio-Hamane, and S. Nakatsuji, "Giant and robust anomalous Nernst effect in a polycrystalline topological ferromagnet at room temperature," Adv. Funct. Mater. **32**, 2206519 (2022).
[17]C. Curcio, E. S. Olivetti, L. Martino, M. Küpferling, and V. Basso, "Study of the temperature dependence of coercivity in MnBi," Phys. Procedia **75**, 1230–1237 (2015).
[18]A. Sola, P. Bougiatioti, M. Kuepferling, D. Meier, G. Reiss, M. Pasquale, T. Kuschel, and V. Basso, "Longitudinal spin Seebeck coefficient: Heat flux vs. temperature difference method," Sci. Rep. **7**, 1–9 (2017).
[19]G. Venkat, C. D. W. Cox, A. Sola, V. Basso, and K. Morrison, "Measurement of the heat flux normalized spin Seebeck coefficient of thin films as a function of temperature," Rev. Sci. Instrum. **91**, 073910 (2020).
[20]B. L. Wooten, K. Vandaele, S. R. Boona, and J. P. Heremans, "Combining spin-Seebeck and Nernst effects in aligned MnBi/Bi composites," Nanomaterials **10**, 2083 (2020).